2000-02

# Kelvin Waves and Internal Bores in the Marine Boundary Layer Inversion and Their Relationship to Coastally Trapped Wind Reversals

Ralph, F. M.; Neiman, P. J.; Wilczak, J. M.; Persson, P. O. G.; Bane, J. M.; Cancillo, M. L.; Nuss, W.

American Meteorological Society

Ralph, F. M., et al. "Kelvin waves and internal bores in the marine boundary layer inversion and their relationship to coastally trapped wind reversals." Monthly weather review 128.2 (2000): 283-300.
http://hdl.handle.net/10945/68841

# Kelvin Waves and Internal Bores in the Marine Boundary Layer Inversion and Their Relationship to Coastally Trapped Wind Reversals

F. M. RALPH,* P. J. NEIMAN,* P. O. G. PERSSON,+ J. M. BANE,# M. L. CANCILLO,@ J. M. WILCZAK,* AND W. NUSS&

* *NOAA/Environmental Technology Laboratory, Boulder, Colorado*
+ *NOAA/CIRES, University of Colorado, Boulder, Colorado*
# *Marine Sciences Program, University of North Carolina, Chapel Hill, North Carolina*
@ *Department of Physics, University of Extremadura, Badajoz, Spain*
& *Department of Meteorology, Naval Postgraduate School, Monterey, California*

(Manuscript received 29 January 1998, in final form 28 January 1999)

ABSTRACT

Detailed observations of a coastally trapped disturbance, or wind reversal, on 10–11 June 1994 along the California coast provide comprehensive documentation of its structure, based on aircraft, wind profiler, radio acoustic sounding system, and buoy measurements. Unlike the expectations from earlier studies based on limited data, which concluded that the deepening of the marine boundary layer (MBL) was a key factor, the 1994 data show that the perturbation was better characterized as an upward thickening of the inversion capping the MBL. As the event propagated over a site, the reversal in the alongshore wind direction occurred first within the inversion and then 3–4 h later at the surface. A node in the vertical structure (defined here as the altitude of zero vertical displacement) is found just above the inversion base, with up to 200-m upward displacements of isentropic surfaces above the node, and 70-m downward displacements below.

Although this is a single event, it is shown that the vertical structure observed is representative of most other coastally trapped wind reversals. This is determined by comparing a composite of the 10–11 June 1994 event, based on measurements at seven buoys, with surface pressure perturbations calculated from aircraft data. These results are compared to the composite of many events. In each case a weak pressure trough occurred between 2.4 and 4.0 h ahead of the surface wind reversal, and the pressure rose by 0.32–0.48 mb between the trough and the wind reversal. The pressure rise results from the cooling caused by the inversion's upward expansion.

The propagation and structure of the event are shown to be best characterized as a mixed Kelvin wave–bore propagating within the inversion above the MBL, with the MBL acting as a quasi-rigid lower boundary. If the MBL is instead assumed to respond in unison with the inversion, then the theoretically predicted intrinsic phase speeds significantly exceed the observed intrinsic phase speed. The hybrid nature of the event is indicated by two primary characteristics: 1) the disturbance had a much shallower slope than expected for an internal bore, while at the same time the upward perturbation within the inversion was quasi-permanent rather than sinusoidal, which more closely resembles a bore; and 2) the predicted phase speeds for the ''solitary'' form of nonlinear Kelvin wave and for an internal bore are both close to the observed intrinsic phase speed.

## 1. Introduction

Coastal regions along the eastern boundaries of oceans are often characterized by oceanic upwelling and a well-defined marine atmospheric boundary layer (MBL) that is capped by a temperature inversion during the warm season (e.g., Neiburger et al. 1961; Gill 1982; Beardsley et al. 1987; Winant et al. 1988). The relative thinness and strength of the MBL inversion, which is on the order of 10°C over 500 m, has been used often to justify application of the shallow-water system of equations to this environment. In these studies the basic state is perturbed by a hypothetical larger-scale process in which coastal mountains either block the cross-shore winds or force the flow to subside in their lee (e.g., Gill 1977; Winant et al. 1988; Rogerson and Samelson 1995; Samelson and Rogerson 1996). The response of the shallow layer to this forcing can include coastally trapped Kelvin waves, density currents, internal bores, and ageostrophic accelerations associated with alongshore pressure gradients. Similarities between disturbances generated under these idealized conditions and those associated with real weather events along the United States west coast during summer have been noted in several studies. However, it remains unclear which of these mechanisms is primarily responsible for the key characteristics of observed disturbances. The observed disturbances are characterized by a reversal of the along-

*Corresponding author address:* Dr. F. Martin Ralph, NOAA/ERL/ETL, Mail Code R/E/ET7, 325 Broadway, Boulder, CO 80303.
E-mail: fralph@etl.noaa.gov

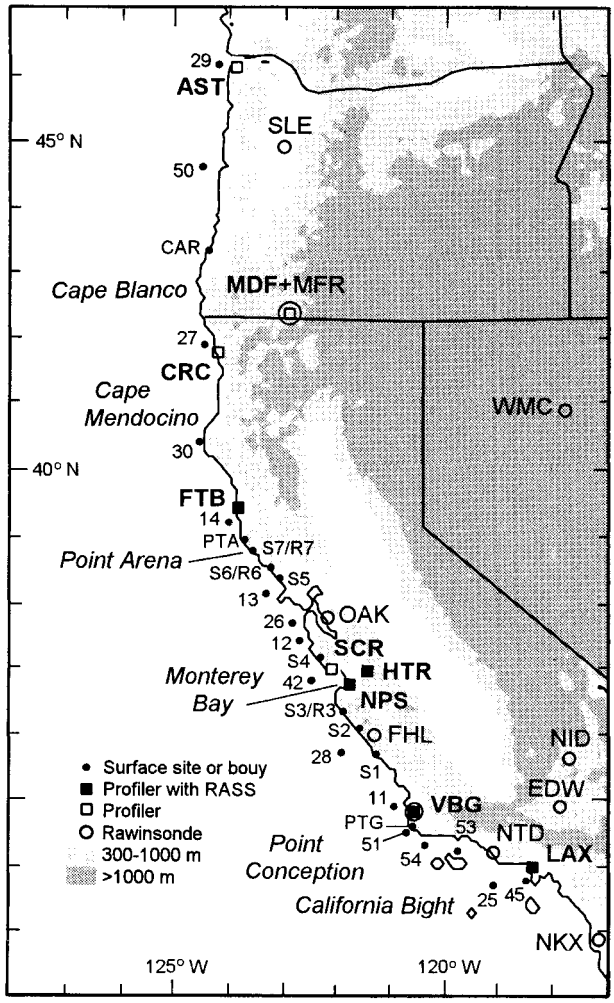


FIG. 1. Base map showing key operational and experimental observing sites and terrain features for the coastal meteorology experiment during the summer of 1994. Buoy numbers XX used here all represent buoys numbered 460XX by NDBC.

shore wind within roughly 100 km of the coast, and with the onset of low clouds or fog. They are referred to here as coastally trapped wind reversals, or more generally as coastally trapped disturbances (CTDs). CTDs are a major forecast problem along the U.S. Pacific coast.

The disturbances that develop in the shallow-water system are characterized by changes in the depth of the MBL, for which early observational studies seemed to lend support (e.g., Gill 1977; Dorman 1985, 1987; Mass and Albright 1987; Hermann et al. 1990). However, partly because of limitations in the ability of operational meteorological measurements to document important aspects of CTDs, a field campaign was carried out to study the origins and dynamical characteristics of these disturbances. The experimental observing system is described in Ralph et al. (1998) and is illustrated here with a base map (Fig. 1). Initial results from this field program have brought into question the applicability of the shallow-water system because observations (Ralph et al. 1998) and mesoscale numerical simulations (Thompson et al. 1997) of the key event, which occurred on 10–11 June 1994 along the California coast, showed that the perturbation was most pronounced within the MBL inversion, the very layer that shallow-water theory assumes to be infinitely thin. Unlike Ralph et al. (1998), which focused on describing the evolving synoptic environment and the CTD's structure, this paper explores the dynamical nature of the event and suggests a method for reconciling the observed three-layer structure with the shallow-water model. Because much of the research from the field experiment has focused on one key event [which did have spatial and temporal scales as well as perturbation amplitudes in wind and pressure that were characteristic of the composite CTDs described by Bond et al. (1996)], this study will also assess how representative the complex, observed, vertical structure of the 10–11 June 1994 event is to most CTDs. However, this study focuses only on the propagating phase of the disturbance and does not examine its initiation.

The primary dynamical mechanisms that have been proposed to explain CTD propagation and structure will be summarized (section 2) and explored, with special emphasis on the role of internal bores and Kelvin waves. The perturbation's synoptic and mesoscale environment are summarized in section 3. The CTD's vertical structure is highlighted (section 4) so as to clearly and accurately illustrate that the MBL inversion was the focus of the disturbance, and that the MBL was perturbed in a sense opposite to that expected from earlier studies. The observed ground-relative propagation of the CTD is summarized, and the possible influence of ambient flow on the intrinsic phase speed is estimated so as to allow comparison with the intrinsic phase speeds calculated from theory (section 5). Coastal buoy data, research aircraft data, and the composite of strong CTDs provided by Bond et al. (1996) are then used to explore the surface manifestations of the multilayered structure, and to establish that the 10–11 June 1994 CTD had a vertical structure that is likely representative of most CTDs in the area (section 6). The observed conditions associated with the CTD, both ambient and perturbed, are then used to calculate the intrinsic phase speeds for Kelvin waves and bores assuming that either the MBL and its inversion responded together or that the MBL acted as a rigid lower boundary (section 7). The results are summarized in section 8, where it is concluded that the 10–11 June 1994 CTD is best characterized as a mixed Kelvin wave–bore that propagated on the MBL inversion and that the MBL acted as a quasi-rigid lower boundary.

## 2. A brief review of Kelvin waves, bores, and density currents

### *a. Atmospheric Kelvin waves*

Coastally trapped Kelvin waves and their possible relationship to CTDs have been the focus of several

studies (e.g., Gill 1977, 1982; Dorman 1985; Beardsley et al. 1987; Winant et al. 1988; Reason and Steyn 1988, 1992, 1995; Rogerson and Samelson 1995; Skamarock et al. 1996; Samelson and Rogerson 1996). These waves are characterized by an alongshore undulation of the depth of the MBL. The alongshore winds within the MBL vary sinusoidally with distance in the alongshore direction, are in geostrophic balance with the cross-shore pressure gradient, and are in phase with the perturbation depth. No significant temperature change necessarily occurs at the surface. Perturbations decay exponentially with distance offshore. Propagation is in the alongshore direction with the coastal barrier to the right of the direction of propagation. Propagation results from the pattern of alongshore horizontal divergence and convergence associated with the wave.

Recent debate (Mass 1995; Reason and Steyn 1995) suggests that Kelvin waves most likely exist within the MBL, but that the relatively small amplitude pressure changes they are expected to produce are difficult to distinguish from the larger-scale changes that they are embedded within, and thus their significance to CTDs in general is unclear. However, recent idealized simulations, using a linear shallow-water model perturbed by realistic forcing based on the climatology of Mass and Bond (1996), has illustrated that these waves do form and that the alongshore momentum balance has a Kelvin wave response that is stronger than the alongshore surface pressure gradient effects (Samelson and Rogerson 1996).

### *b. Atmospheric internal bores and density currents*

In contrast to the gradual transitions associated with Kelvin waves, atmospheric internal bores (e.g., Houghton and Kasahara 1968; Rottman and Simpson 1989; Klemp et al. 1997), and density currents (e.g., Benjamin 1968; Simpson 1987) are characterized by sharp transitions, or jumps, which some studies have related to CTD behavior (Dorman 1987; Mass and Albright 1987; Beardsley et al. 1987; Hermann et al. 1990). Klemp et al. (1997) recently developed a theory for which the predicted propagation speed of an internal bore converges to that of a density current when the depth of the lower layer ahead of the bore approaches zero. The propagation of bores depends on the depth of the lower layer ahead of and behind the jump, as well as on the densities of the upper and lower layers. Density current propagation speed depends on the depth of the dense fluid, and on the density contrast between it and the ambient environment. The proper asymptotic behavior where the propagation speed of a bore converges to that of a density current depends on the assumption that energy loss occurs in the upper layer for both the density current (Benjamin 1968) and the bore (Klemp et al. 1997). There are two important distinctions between a bore and a density current that are relevant to this study: 1) in the case of a density current the denser fluid must travel at least as fast as the leading edge of the density current, while for a bore the fluid flows through the jump; and 2) for an observer at the surface there is no temperature change with a bore, but there is with a density current.

Although Mass and Albright (1987) showed that a strong event they studied had characteristics of a density current, the later climatological study by Bond et al. (1996) concluded that event was the strongest in the entire 10-yr period of their study, thus questioning its representativeness to most events. Ralph et al. (1998) concluded that the key aspects of the event studied here were inconsistent with density current behavior; that is, propagation exceeded the maximum wind speeds in the direction of propagation, the wind shift was gradual, and the temperature rose after the wind shift. For these reasons the density current mechanism is not analyzed further in this paper. However, Thompson et al. (1997) did conclude that their mesoscale simulation of the 10–11 June 1994 event did contain a period where the simulated behavior had some characteristics of a density current.

### *c. Ambiguities and distinguishing factors*

When the amplitude of vertical displacements in a Kelvin wave becomes a substantial fraction of the depth of the lower layer, nonlinear effects can become important and the disturbance can propagate faster than it would as a linear Kelvin wave. In general, nonlinear waves can steepen, possibly forming a borelike or density current–like leading edge, unless the nonlinearities are balanced by dispersion. If this balance is assumed, theory yields the special solitary wave solution, including a relationship for the propagation phase speed (Reason and Steyn 1992). Although it has not been established that dispersive effects balance the nonlinearities in Kelvin waves, Reason and Steyn (1992) showed that such a balance would allow a linear Kelvin wave to steepen into a solitary Kelvin wave over roughly two days under their idealized conditions. The speed of a linear Kelvin wave is less than that of a solitary Kelvin wave, which is less than that of an internal bore, which is less than or equal to that of a density current. Also, a bore is steeper than a pure solitary Kelvin wave, which is steeper than a linear Kelvin wave. While a bore is traditionally viewed as a single sudden deepening of the fluid, Kelvin waves are usually considered as more wavelike, but they can also be described by a hyperbolic tangent profile as shown in Fig. 1 of Skamarock et al. (1996). Thus, the propagation speeds and the structure of these disturbances may be useful in determining which mechanisms are responsible for the observed behavior.

## 3. The synoptic and mesoscale environment of the CTD

The synoptic-scale environment of this event is described in detail in Ralph et al. (1998) and in most

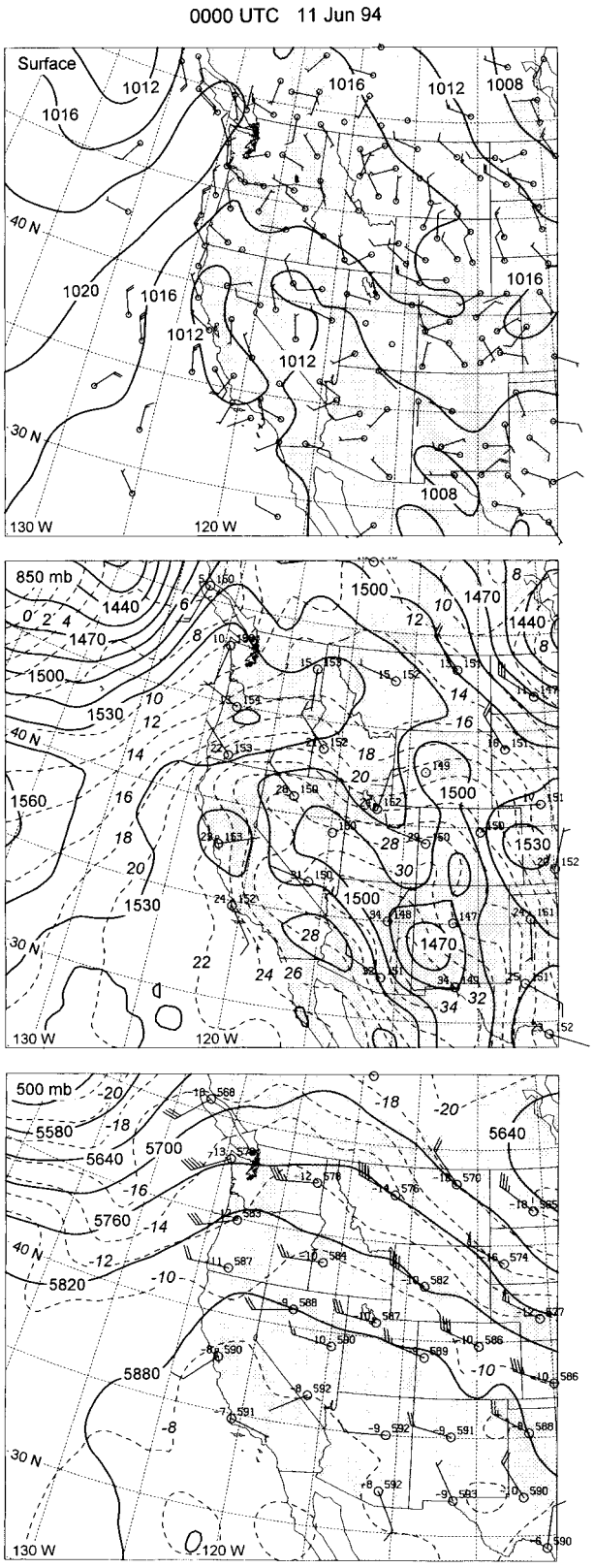


FIG. 2. Synoptic conditions at the surface, 850 mb, and 500 mb. Surface station plots show wind velocities (half barb = 2.5 m $s^{-1}$; full barb = 5 m $s^{-1}$; flag = 25 m $s^{-1}$). Upper level station plots show winds (as at the surface), temperature (°C; upper left), and geopotential height (dm; upper right). Automated sea level pressure analyses (solid; contoured every 4 mb) are shown on surface charts. Automated geopotential height analyses (solid; contoured every 15 and 60 m, at 850 and 500 mb, respectively), and temperature analyses (dashed; contoured every 2°C) are shown at upper levels. These analyses are from a data assimilation technique using multiquadric interpolation (Nuss and Titley 1994) at each analysis time, which includes the experimental data and NCEP's Eta Model first-guess fields over the ocean.

respects resembles that found in a climatology of many CTDs (Bond et al. 1996; Mass and Bond 1996). However, it will be briefly described here and supplemented by synoptic analyses at the most relevant time for this paper, that is, 0000 UTC 11 June 1994 (Fig. 2). By this time a synoptic-scale ridge at 500 mb had moved into the Pacific Northwest, with its axis crossing the coast before 0000 UTC 11 June (Fig. 2). This suggests that the large-scale subsidence associated with the ridge had been present over the coast during the previous day and that the area of active subsidence had already moved inland. As the ridge moved onshore to the north of California, a region of warm continental air was advected offshore over central California. This warm advection is seen still at 0000 UTC 11 June in the 850-mb analysis near San Francisco (Fig. 2b), which is just north of the leading edge of the CTD. Ralph et al. (1998) showed that this caused warming primarily in the lowest 2 km over the region, which induced 24-h pressure falls at the surface comparable to those that were observed. Thompson et al. (1997) used a numerical simulation to conclude that downslope warming from easterly flow over the coastal ranges could have also contributed. Because this warming was localized along roughly 600 km of the coast, the pattern of pressure falls included a well-defined center, which propagated northward from central California to the Oregon border between 1200 UTC 9 June and 1200 UTC 10 June at an average speed of 7.7 m $s^{-1}$. Over time, these pressure falls associated with warming acted to extend the thermal trough into northern California from its normal position over the deserts to the south, and likely contributed to the formation of a trough of low pressure that extended offshore. At 0000 UTC 11 June, the coastal trough had evolved on the mesoscale into a weak low pressure center roughly 200 km west of the central California coast (Fig. 7e of Ralph et al. 1998). Note, however, that the synoptic-scale mean sea level pressure analyses in Fig. 2, which were created using the multiquadric interpolation routine of Nuss and Titley (1994), smooths over this mesoscale feature. Nonetheless, Fig. 2 still illustrates that this evolution eventually created a region along the coast where the normal alongshore pressure gradient (high pressure to the north) was reversed, or at least nearly zero. This is characteristic of conditions found in other CTDs (Mass and Albright 1987; Bond et al. 1996; Mass and Bond

1996) and was enhanced by rising pressures in the California Bight (approximately 2 mb over 24 h). In short, this synoptic-scale evolution created a region of weak alongshore pressure gradient that helped weaken the climatologically normal northerly winds, which allowed the developing CTD to propagate northward.

## 4. The perturbation vertical structure observed in the 10–11 June 1994 CTD

During the CTD event of 10–11 June 1994 a twin-engine, instrumented aircraft (Bane et al. 1995) measured conditions offshore using a vertical sawtooth flight pattern 225 km long that headed southward, paralleling the coast, from the region of northerlies to the region of southerlies. This track crossed the northern edge of the low clouds (Fig. 3a). [The coast is not oriented truly north–south, but rather, it is roughly 150° to 330°. Thus the terms southerly and northerly are used here to refer to the alongshore wind component (U); $U > 0$ is southerly flow.] The track extended from where the buoy array indicated the pressures were lowest along the coast at that time, which was 1012.1 mb at buoy 26 between the mouth of San Francisco Bay and Point Arena [see the analysis in Fig. 7e of Ralph et al. (1998)]. Just to the north of this buoy the pressure was 1012.4 mb at buoy 13, and to its south it was 1012.7 mb. All three of these buoys were located almost directly beneath the flight track in Fig. 3a. This weak trough is roughly 100–150 km north of the surface wind shift, as seen in the aircraft cross section (Fig. 3b). The 3-h pressure tendencies along the coast were all between $-0.1$ and $-1.0$ mb from southern California to Washington (not shown). There was no clear alongshore variation of this variable, and the pressure falls were likely part of the diurnal or semidiurnal atmospheric tides.

The vertical cross section (Fig. 3b) establishes that the perturbation was characterized primarily as an upward expansion of the MBL inversion, with strong evidence that southerlies appeared first within the MBL inversion and then at the surface, as is described by Ralph et al. (1998). This conclusion is possible partly because of the favorable positioning of the flight track over four buoys and the ship *Glorita*. It is also apparent that the vertical sampling, which was roughly every 3–10 m, adequately resolved the fine vertical structure of the MBL inversion, and enough alongshore vertical profiles were performed that the alongshore structure is also well resolved. In short, the aircraft measured the ambient and perturbed regions of the MBL inversion with spatial resolutions that were adequate to capture key vertical and alongshore structures, unlike data from earlier studies. These data also have the distinct advantage that the observed perturbation is relatively far removed from local effects such as those arising from headlands.

To more quantitatively illustrate the vertical structure of the thermodynamic perturbation, the raw vertical profiles of aircraft potential temperature data from the ambient and perturbed portions of the cross section in Fig. 3b are shown (Fig. 4). These correspond to ascent profiles labeled 1 and 3 in Fig. 3b. Even though profile 4 is positioned somewhat better than profile 3 for this purpose, that is, both the wind and temperature perturbations are strongest there, profile 3 is used for the thermodynamic variables. This is done because there was evidence of hysteresis in the aircraft temperature data that was eliminated by using two ascent profiles, rather than an ascent profile and a descent profile. Profile 4 is still used for calculating the perturbation of the alongshore wind, because it is more representative of the fully perturbed momentum field. Vertical profiles of perturbation temperature, perturbation alongshore wind, and vertical displacement of isentropes were then derived from these aircraft soundings (Fig. 5). The vertical profiles used are from positions that were roughly 140 km apart, with the northernmost ascent interpreted as the ambient profile because the flow was northerly throughout. The vertical displacement was measured from the change in altitude of potential temperature levels from the ambient profile, under the reasonable assumption of adiabatic motion (the profiles were from outside the cloudy region). The altitude of a value of the vertical displacement derived in this way was plotted in Fig. 5 as occurring at the altitude the isentrope was at in the ambient environment. From this comparison in Figs. 4 and 5, it is evident that very little changed above 950 m above mean sea level (MSL). However, the MBL inversion cooled by up to 4.4°C in the layer from 265 to 950 m and warmed by up to 2°C below that. A 0.2°C warming was also evident in the surface data, which is shown later to be consistent with observations at several buoys. Upward vertical displacements of some isentropes exceeded 200 m within the MBL inversion, and downward displacements are estimated as 70 m within the MBL. While the thermodynamic perturbations had greatest amplitude in the MBL inversion, the kinematic perturbation to the alongshore wind was generally strongest at lower altitudes, with the maximum value located at the base of the inversion and very small perturbations ($<2$ m s$^{-1}$) in the upper part of the inversion above 500 m MSL (Figs. 5 and 6a). In contrast, the kinematic perturbation to the cross-shore wind was small in the MBL, and larger in the inversion (Fig. 6b).

The appearance of southerly flow, first in the MBL inversion, and then at the surface, is highlighted in Fig. 6a, which also shows that most of the wind shift at that level occurred within 60 km in the alongshore direction. This region where surface winds were still northerly, even though winds had become southerly within the inversion, is referred to as the ''transition'' zone in Fig. 6. The initial development of southerlies within the inversion aloft cannot be explained as resulting from the vertical profile of the diurnal cycle of the northerly alongshore jet, because this diurnal jet is maximized within the inversion, rather than at the surface (Holt 1996). The alongshore winds reversed only in the lowest

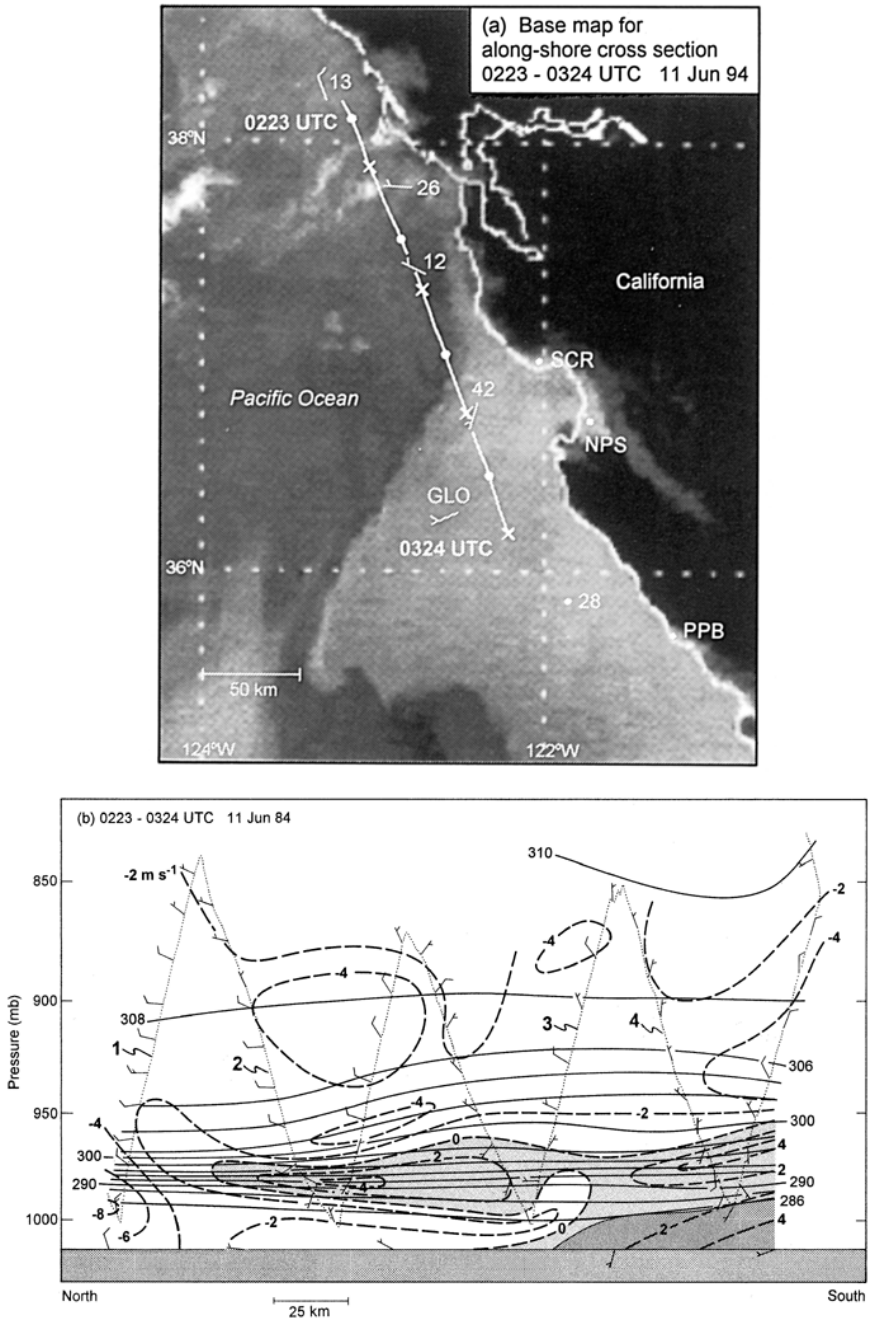


FIG. 3. (a) Infrared satellite image at 0336 UTC 11 Jun 1994 showing the Piper research aircraft's flight track between 0223 and 0324 UTC 11 Jun that was incorporated into the cross section in (b). The dots and ×s denote the bottoms and tops of the sawtooth flight track, respectively. Wind velocities from offshore buoys (42, 12, 26, and 13) and the ship *Glorita* (*GLO*) are shown. The locations of buoy 28 and the 915-MHz wind profilers at the Naval Postgraduate School (NPS), Piedras Blancas (PPB), and Santa Cruz (SCR) are also marked. (b) Cross section of potential temperature (K, solid) and alongshore (330°–150° orientation) wind speed (m $s^{-1}$, bold dashed; >0 is southerly and shaded lightly) using data between 0223 and 0324 UTC 11 Jun 1994 from the flight track shown in (a). Selected wind velocities along the flight track (dotted) are shown. The dark shading above the sea surface marks the region of low clouds. Selected profiles are marked 1 through 4 from north to south, respectively. Wind velocities in both panels are as in Fig. 2. [Adapted from Ralph et al. (1998).]

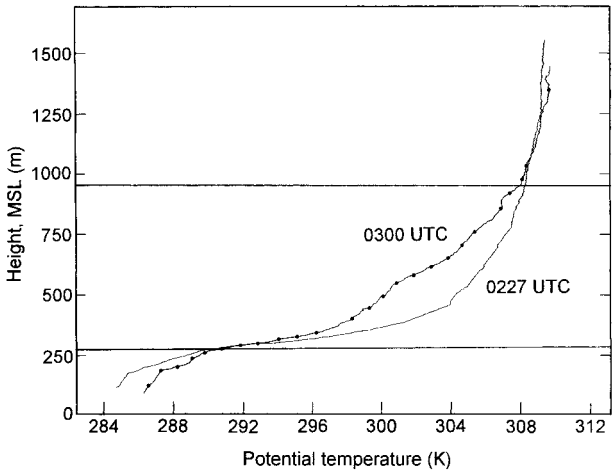


FIG. 4. Aircraft soundings of potential temperature (K) at 0227 UTC (profile 1 in Fig. 3b) and 0300 UTC (profile 3 in Fig. 3b) 11 Jun 1994 from the Piper research aircraft. The two bold horizontal lines mark the layer containing the primary disturbance above the marine boundary layer.

350 m, but changed by up to 10 m $s^{-1}$ in that layer (Figs. 5 and 6a). The cross-shore wind changed by up to 6 m $s^{-1}$, with onshore flow in the ambient environment and offshore flow south of the position of the alongshore wind reversal (Fig. 6b). It is clear that the cross-shore wind perturbation is a large fraction of the alongshore wind perturbation; however, it is concentrated at higher altitude.

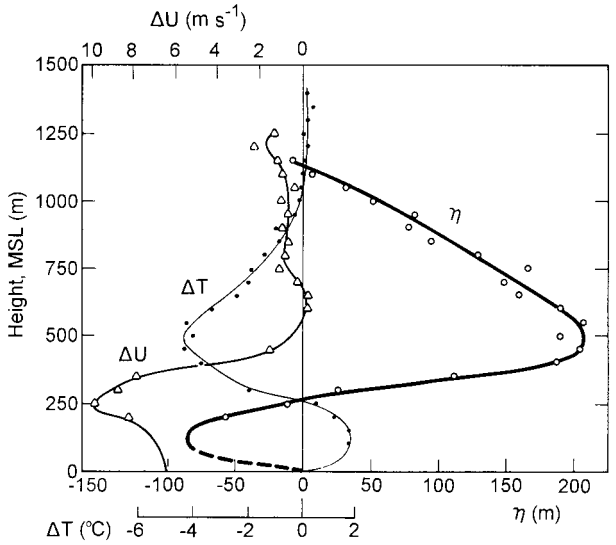


FIG. 5. The difference between the two soundings shown in Fig. 4 (sounding at 0300 UTC minus sounding at 0227 UTC, which are profiles 1 and 3 in Fig. 3b) for temperature ($\Delta T$, °C; thin curve) and vertical displacement of isentropes [$\eta$, m; bold curve (dashed curve is interpolated)]. The difference in alongshore wind speed ($\Delta U$, m $s^{-1}$; medium curve) is based on the difference between profiles 1 and 4 in Fig. 3b. Solid dots, open circles, and open triangles are data points of $\Delta T, \eta$, and $\Delta U$, respectively, that the three curves are based upon.

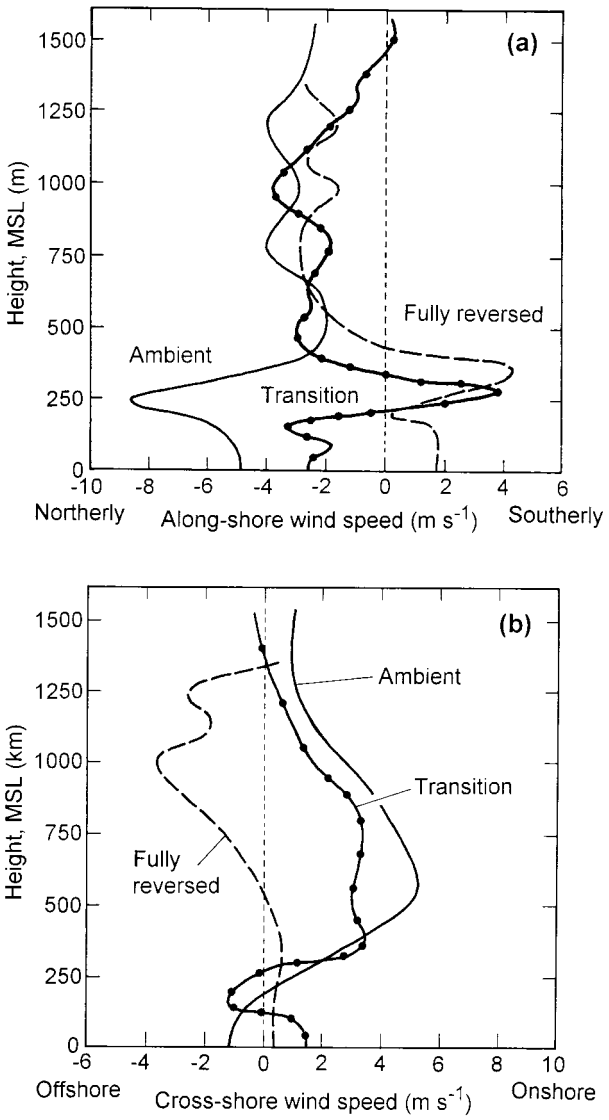


FIG. 6. Profiles of the (a) alongshore and (b) cross-shore wind components (m $s^{-1}$) from profiles 1, 2, and 4 in Fig. 3b. Profiles 1, 2, and 4 are approximately 112 km north (ambient, solid curve), 60 km north (transition, dotted curve), and 60 km south (fully reversed, bold dashed curve) of the location of the shift from northerly to southerly at the surface, i.e., where the 0 m $s^{-1}$ isotach intersects the ocean surface in Fig. 3b.

## 5. Alongshore propagation and the influence of the diurnal cycle

### *a. Overview of observed propagation of the 10–11 June 1994 CTD*

The reversal of the alongshore wind from northerly to southerly, which has traditionally defined a CTD, progressed northward over roughly 30 h, with a 12-h interruption (Fig. 7; also see Fig. 8 of Ralph et al. 1998). Based on this two-phase interpretation of the northward progression, which is consistent with earlier case studies of other events (e.g., Dorman 1985), a very good linear

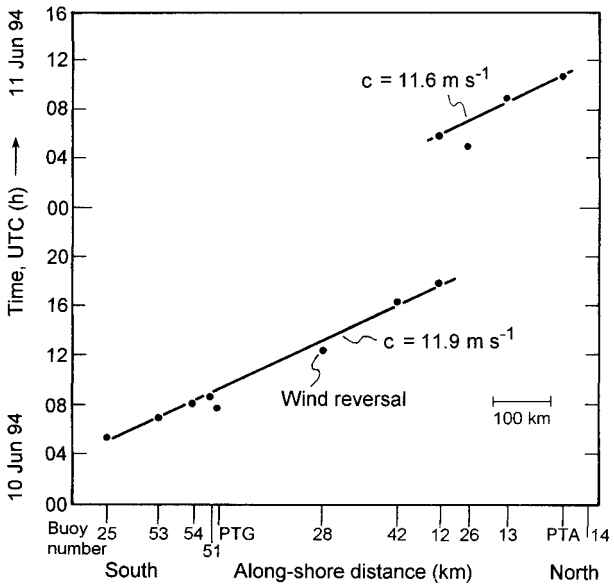


FIG. 7. Time of the observed change in sign of the alongshore wind from northerly to southerly at the surface (solid dots). The speed of northward alongshore progression of the wind reversal during two periods characterized by propagation are given. [Adapted from Ralph et al. (1998).]

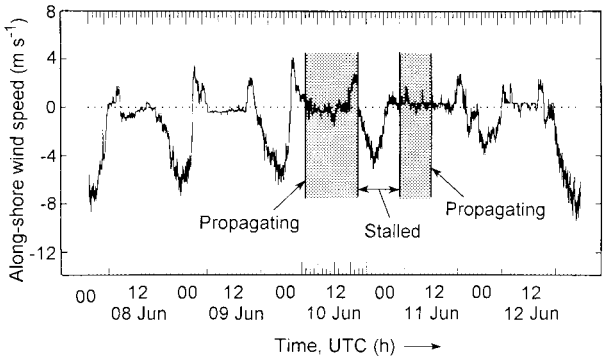


FIG. 8. Time series of 1-min resolution alongshore surface wind speed (m $s^{-1}$) measured at the SCR 915-MHz wind profiler between 0000 UTC 8 and 13 Jun 1994. The two shaded regions correspond to the periods when the coastally trapped disturbance propagated northward, and the area between them marks the period when the disturbance was stalled.

fit is found for buoys between Palos Verdes (buoy 25) and just north of Monterey Bay (buoy 12) on 10 June. (Buoy numbers given here as XX represent the full buoy number 460XX, and their locations are marked in Fig. 1.) The calculated phase speed is 11.9 ± 0.3 m $s^{-1}$, where the uncertainty is based on calculations excluding points that may be influenced by other behavior as described by Ralph et al. (1998). After the 12-h pause, southerlies progressed north of Monterey Bay, reaching their farthest northern extent near Point Arena (PTA coastal site).

This propagation is much faster than the 7.7 m $s^{-1}$ northward movement over 24 h of the center of strongest sea level pressure falls along the coast, which is associated primarily with the evolving synoptic-scale conditions as described in section 3. However, if the 12-h pause in its northward propagation is ignored and the speed is calculated from Fig. 7 over 24 h, the 24-h average propagation speed of the CTD is 6.1 m $s^{-1}$, which is closer to the speed of movement of the synoptic-scale pressure fall center. Although this suggests that the propagation of the CTD was more closely tied to changes in the synoptic scale, it is still difficult to reconcile why the CTD would have paused, given that the synoptic-scale evolution should not be so discontinuous. The fact that many CTDs exhibit this pause, which is normally related to the diurnal cycle of alongshore winds (as is described in the next section), indicates that this inconsistency is present in many other events as well. Thus, it appears that synoptic conditions set the stage for the CTD, which then propagated along the coast, somewhat independent of the more slowly evolving synoptic-scale conditions.

### *b. The magnitude and timing of the diurnal cycle in alongshore wind*

#### 1) THE DIURNAL CYCLE AT THE SURFACE

Northward progression of the CTD began at roughly 0500 UTC (2200 local daylight time) on each day. The pause occurred during the phase of the diurnal cycle normally characterized by increased northerly flow (Beardsley et al. 1987), which would have opposed any northward-propagating disturbance within the MBL. This conjecture, which has traditionally been used to explain such pauses, is supported by the time series of alongshore winds at Santa Cruz (SCR), which is a coastal site in the vicinity of the pause (Fig. 8). Because it is on the coast, the site should be expected to experience the maximum, or near-maximum, effects of the diurnal cycle, and thus it provides a sensitive measure of the diurnal cycle. [While the maximum diurnal variation is normally at the coast (Beardsley et al. 1987; Winant et al. 1988), it can be found up to 12 km offshore (Winant et al. 1988).] This site exhibited a pronounced diurnal cycle of alongshore winds of 9.6–10.5 m $s^{-1}$ (peak to peak) averaged over 4–6 days surrounding the CTD, with the average time of maximum winds at 2245 UTC, minima at 0430 and 1545 UTC, and very weak winds from 0400 to 1600 UTC each day. The timing of this diurnal cycle is very similar to the climatological part of the study by Beardsley et al. (1987), which had maximum winds at 2200–2300 UTC and a broad minimum from 0500 to 1600 UTC. This broad minimum corresponded to the interval with winds that were less than 1.7 m $s^{-1}$ stronger than the minimum winds during the diurnal cycle and at least 7 m $s^{-1}$ weaker than the maximum winds.

The magnitude of the diurnal cycle of alongshore

wind at SCR is close to that of the week-long period documented by Beardsley et al. (1987) for which the diurnal cycle had its greatest amplitude during their experiment (8.5 m $s^{-1}$ peak to peak). Based on data provided in Winant et al. (1988), it was also possible to calculate the average diurnal cycle over two weeks centered on the same date as the 1994 CTD, but from a 1982 field experiment. On average, the alongshore wind varied by 5.5–10.8 m $s^{-1}$ each day during that period. The strongest variation was at a buoy 12 km offshore; the weakest at a buoy 30 km offshore, with a 7.3 m $s^{-1}$ variation at the coast. In contrast, Beardsley et al. (1987) concluded that the diurnal cycle tends to decrease with increasing distance offshore and suggested that the light (or calm) winds within the MBL over the coast at night extend typically to about 20 km offshore. However, inspection of the detailed time series indicates that their data also included significant periods during which the diurnal cycle amplitude did not decrease substantially within 30 km offshore. Thus, the earlier studies indicate that the diurnal cycle can be strongest offshore. In the case of the 10–11 June 1994 CTD studied here, this implies that the diurnal cycle offshore could have been greater than the approximately 10 m $s^{-1}$ value observed at the coast and, thus, could have been sufficiently strong so as to completely stop the 11.9 m $s^{-1}$ northward propagation of the CTD.

#### 2) The vertical extent of the diurnal cycle: Characteristics based on a 1-month composite from wind profiler data

Because it is unclear whether the strong diurnal cycle observed at the surface extends upward throughout the layer in which the CTD propagated (at least to 950 m MSL), an attempt was made to measure the diurnal cycle aloft. However, the profiler sites in the region through which the CTD propagated during the 1994 field experiment were not well suited for this. They were very near Monterey Bay, where the diurnal cycle may be substantially different than that along most of the coast. This arises because Monterey Bay modifies the local coastal circulations significantly, and there is a strong connection to the San Joaquin Valley through a major gap in the coastal mountains (Banta 1995). To overcome this limitation, data were used from the ideal location for the 1994 CTD, but collected in 1996, when such data were available. The site is located along the same portion of the coast where the 1994 CTD exhibited its most systematic propagation and is near the center of the coastal area over which it propagated. During the summer of 1996 a wind profiler was located at Point Piedras Blancas along the Big Sur coast, which is 120 km south of Monterey, much farther away from the strong influence of Monterey Bay. The period between 24 June and 21 July 1996 was used because of the excellent data quality and vertical coverage from 150 to 2300 m MSL available during that period. After carefully editing the hourly consensus averaged winds for interference and gross errors, measurements were available for >90% of all times at all heights below 1.2 km MSL. The data were then used to create a composite of the winds as they varied through their diurnal cycle (Fig. 9) based on 25–28 samples at each height and time. The alongshore wind speed at 100 m MSL varies from −8 m $s^{-1}$ near 0200 UTC each day (1900 LDT) to −1.5 m $s^{-1}$ near 1700 UTC (1000 LDT). This strong diurnal variation extends over most of the layer in which the CTD perturbation was observed, although the magnitude of the diurnal variation decreases with height. Using the interval between 0600 and 1800 UTC during which the CTD propagated, and the layer below 1.2 km MSL in which it propagated, a mean alongshore wind speed of −1.4 m $s^{-1}$ (northerly) was calculated from the data. This procedure was also performed on two 10-day subperiods (24 June–3 July and 12–21 July) within this 28-day period to assess the variability of this estimate. Each one also had an average of −1.4 m $s^{-1}$. Further, by eliminating the period from 0600 to 0900 UTC, the average changed to −1.0 m $s^{-1}$. Based on these three samples and on their sensitivity to the time interval selected, it is reasonable to suggest that the average alongshore flow in the region through which the CTD propagated in 1994 was −1.3 ± 0.3 m $s^{-1}$.

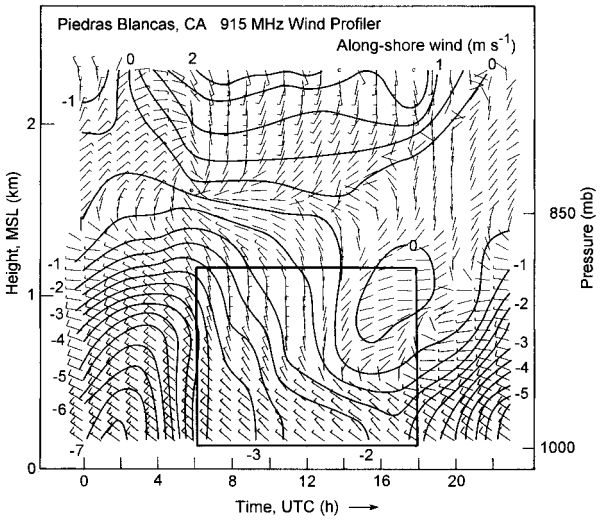


FIG. 9. A month-long composite of the diurnal behavior of the alongshore wind speed (m $s^{-1}$) measured by the Piedras Blancas, CA, 915-MHz wind profiler from 24 Jun through 21 Jul 1996 (the location is marked in Fig. 3a). The inner box defines the approximate vertical and temporal bounds of the propagating phase of the coastally trapped disturbance of 10–11 Jun 1994. Southerly flow is less than 0 m $s^{-1}$. Wind vectors are as in Fig. 2.

### *c. Estimation of the intrinsic phase speed of the CTD on 10–11 June 1994*

The analyses presented in this section indicate that the alongshore wind went through a diurnal cycle of

approximately 10 m $s^{-1}$ at a surface site during the 10–11 June 1994 CTD, and that this magnitude of diurnal cycle of the alongshore wind has been documented in earlier studies as well. The peak northerly flow during this diurnal variation is almost strong enough to halt the northward ground-relative propagation of the CTD (11.9 m $s^{-1}$) along the coast. A similar, although somewhat weaker, diurnal variation was found throughout the lowest 1.2 km MSL in the same region through which the CTD propagated. It also indicates that the maximum diurnal alongshore winds opposite to the CTD propagation occurred near the center of the CTD pause (0000 UTC), and that the broad 12-h minimum in alongshore opposing winds corresponds to the period when propagation occurred (0600–1800 UTC).

These data suggest that the best estimate of the ambient alongshore flow during the period of CTD propagation is $-1.3 \pm 0.3$ m $s^{-1}$. This is an average over the layer in which the CTD propagated. Because this flow would have opposed the ground-relative propagation of the CTD, it is concluded that the CTD's intrinsic phase speed was $13.2 \pm 0.6$ m $s^{-1}$.

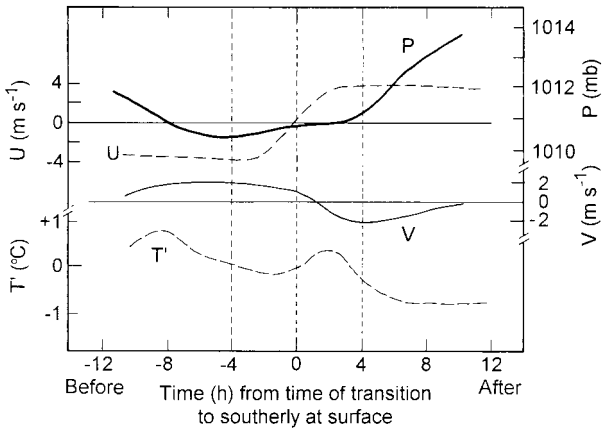


FIG. 10. Composite system-relative time series of alongshore wind ($U$, m $s^{-1}$), cross-shore wind ($V$, m $s^{-1}$), pressure ($P$, mb), and perturbation temperature ($T'$, °C), calculated from those buoys (see text) that experienced the 10–11 June 1994 coastally trapped disturbance. The composite is centered relative to the time of the alongshore wind reversal from northerly to southerly (i.e., $U = 0$ m $s^{-1}$ at time = 0 h).

## 6. Evidence that the observed vertical structure of the 10–11 June 1994 CTD is representative of other CTDs

### *a. Creation of the composite time series for the 10–11 June 1994 CTD from buoy data*

Coastally trapped disturbances traditionally have been studied using hourly data from ~20 operational data buoys moored 15–30 km offshore. For example, they were used in the previous section to measure the northward propagation of the CTD of 10–11 June 1994. To determine the general sequence of events encountered by each of the buoys that experienced this CTD, a composite of the evolution relative to the time of the alongshore wind reversal at each buoy was calculated (Fig. 10). This approach is similar to that used by Bond et al. (1996) to study many CTDs at a specific buoy, except that it is applied to the evolution of a specific CTD at several buoys.

The key to creating a composite that accurately represents a particular phenomenon is recognizing which events are too weak to include in the composite, or which are adversely influenced by other phenomena that could confuse the signal. It is essentially a signal-to-noise problem. In this case the number of data points is limited, so it is critical to properly select which buoys to include in the composites. Site selection was initially based on whether the site experienced a well-defined reversal in the alongshore wind component (see Fig. 8 of Ralph et al. 1998). Although buoy 26 experienced a wind reversal, it appeared to be strongly influenced by diurnal effects likely resulting from its proximity to the mouth of San Francisco Bay and so was excluded from the composites. PTA was excluded because it was at the northern terminus of the CTD, where the southerlies were only briefly present. Buoy 12 was also excluded because the time series at that site was confused by the pause in the CTD's northward propagation that occurred near that site (Fig. 7). Buoys 25, 54, 51, PTG, 28, 42, and 13 all experienced a well-defined alongshore wind reversal and, thus, form the sites used to create the composite. However, some sites were excluded from the composite for a particular variable. Pressure data was missing at buoy 42, and the cross-shore component there was dominated by diurnal effects likely related to its position at the mouth of Monterey Bay. An eddy in the lee (north) of Point Conception during the southerly flow dominated the cross-shore winds at PTG (Ralph et al. 1998). Thus, the composites for each variable are based on five to seven sites where the perturbation was well defined. As described in the detailed comparison below, the major features in the event composite (Fig. 10) are similar to those found in the composite of many strong CTDs at buoys 28 and 13 (Bond et al. 1996). This indicates that the data selection used here was appropriate.

### *b. Summary of the 10–11 June 1994 event composites and comparison with the CTD climatological composites of Bond et al. (1996)*

Several important features are immediately evident from the event composite (Fig. 10). The alongshore wind shifted by 7.8 m $s^{-1}$ over 6–8 h from steady northerly to steady southerly in a nearly hyperbolic tangent manner. For comparison, the buoy 28 climatology of Bond et al. (1996) showed a 9.1 m $s^{-1}$ shift over 9 h. In the 10–11 June 1994 CTD a broad (2–3 h) pressure trough marked the beginning of the decrease in northerly

flow and occurred roughly 3.5 h before the wind reversal, followed by a 0.38-mb pressure rise over 3.5 h. This is quite similar to the climatological results at buoy 28, which showed a 4-h pressure rise of 0.32 mb leading up to the alongshore wind reversal. The Bond et al. climatology at buoy 13 is very similar, with a 3-h pressure rise of 0.48 mb. In fact, the average of this behavior from the climatology of CTDs at buoys 28, 13, 27, and 10 are 3.2 h and 0.52 mb (Bond et al. 1996). The larger pressure rise of 2.4 mb during the 12 h after the alongshore wind reversal in the event composite is also close to the 2.3-mb rise found in the buoy 28 climatology, although the pressure rise is less monotonic in the 1994 event composite. Additional features of the 10–11 June 1994 CTD event composite are the shift from 1.2 m $s^{-1}$ onshore flow in the northerlies before the alongshore wind reversal to 1.2 m $s^{-1}$ offshore flow in the southerlies, and a 0.2°C temperature rise during the 2–3 h after the alongshore wind reversal. Although there is similar behavior in the buoy 28 climatology of cross-shore winds, the temperature change signature in the climatology appears dominated by diurnal effects. This close comparison between the results of the Bond et al. (1996) climatology of many CTDs and the 10–11 June 1994 event indicates that the 10–11 June 1994 CTD was characteristic of many CTDs, at least in terms of perturbations at the surface. These similarities include the weak pressure trough and subsequent rise, and its 3–4-h phase lag before the alongshore wind reversal, as well as the larger pressure rise after the reversal, and the change from onshore- to offshore-directed cross-shore flow.

### *c. Comparison with the perturbation observed on the marine boundary layer inversion*

Because the alongshore variation in surface pressure is a key characteristic of CTDs, Kelvin waves, and bores, and is readily measured at the surface, it is important to consider how the changes in the MBL inversion affected the surface pressure. The availability of detailed vertical temperature profiles from the aircraft, both ahead of and within the perturbation, provides an opportunity to assess this in a accurate and relevant way. Because the observed conditions are characterized by weak vertical motions, estimated to be $<5$ cm $s^{-1}$ from the slope of the isentropes in Fig. 3b and from the 11.9 m $s^{-1}$ phase speed, the hydrostatic assumption is employed to calculate the contribution to surface pressure from the lowest 950 m (the layer that experienced significant temperature changes, as shown in Fig. 4). Subtracting the value calculated from the ambient profile 110 km north of the analyzed surface wind reversal yields perturbation pressures of 0.37, and 0.59, and 0.60 mb at positions $-40$, 30, and 100 km from the surface wind reversal, respectively, where negative values are north of the surface wind reversal. Because the aircraft measurements were not made below 70-m altitude, these calculated surface pressure changes exclude the effects of that layer, even though the analyses suggest slight warming. For reference, when the pressure change calculations included the layer below 70 m the pressure perturbations were 0.32, 0.58, and 0.56 mb at positions $-40$, 30, and 100 km from the surface wind reversal.

TABLE 1. Summary of the observed pressure rise ($\Delta P$) between the surface pressure trough and the reversal of the alongshore wind at the surface, and of the phase lag ($\Delta t$) between them. Results are from aircraft measurements of the upward expanding MBL inversion and the composite of buoy observations during 10–11 Jun 1994 CTD, as well as the average of the climatology of many events over 10 y at buoys 28 and 13 [given in Bond et al. (1996)].

| Data | $\Delta P$ (mb) | $\Delta t$ (h) |
|---|---|---|
| Aircraft | 0.47 | 2.4 |
| Buoy event composite | 0.38 | 3.5 |
| Climatology | 0.40 | 3.5 |

If it is assumed that this perturbation of the MBL inversion also propagated northward across the buoys used in the event composite at the same speed (11.9 m $s^{-1}$) as the alongshore wind reversal at the surface, then the pressure rise of 0.59 mb would have occurred over 3.3 h. After interpolating to the analyzed position of the wind reversal at the surface, these data indicate that there was a pressure rise of 0.47 mb over 2.4 h before the surface wind shift. These aspects are compared in Table 1 with both the magnitude and temporal scale in the event composite in which the pressure rose 0.38 mb over 3.5 h, and in the average climatology from buoys 28 and 13 in which the pressure rose 0.40 mb over 3.5 h. This favorable comparison is brought out graphically in Fig. 11. (Note that the spacing of the surface data within the cross section implies an uncertainty in the exact position of the surface wind reversal relative to the pressure perturbation of $\pm 30$ km, which corresponds to $\pm 0.7$ h.) Overall, results from the event composite and analysis of the aircraft cross section for the 10–11 June 1994 case, and the climatological study by Bond et al. (1996) for buoys 28 and 13, indicate that CTDs in the region are characterized by the passage of a weak surface pressure trough 2.4–4.0 h before the surface wind shift and that the pressure rises by roughly 0.3–0.5 mb between the trough and the wind reversal.

The favorable comparison between the aircraft-derived pressure perturbations and the event composite indicates the assumption that the perturbation of the MBL inversion propagated in connection with the surface wind reversal was justified. (Recall that this assumption was required because aircraft observations were available only while the CTD's northward propagation was stalled.) Because the pressure signature is also characteristic of most CTDs in the region, these results also indicate that the perturbed MBL inversion observed in the 10–11 June 1994 event is characteristic of most CTDs in the region. Although it is possible that some other mechanism could have created a similar sur-

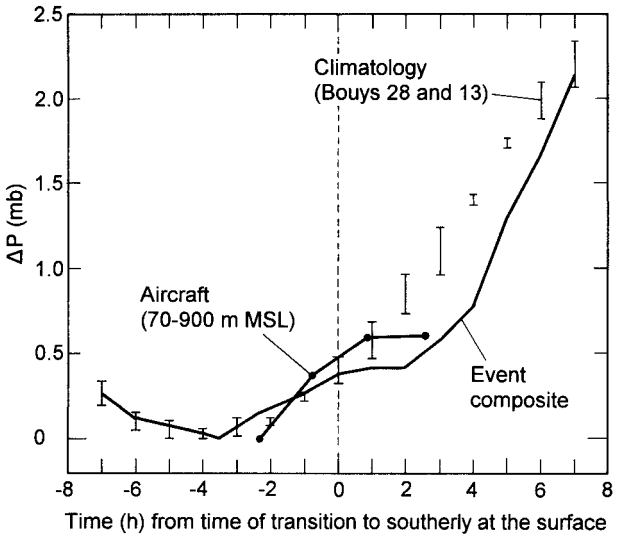


FIG. 11. Three independently derived sea level pressure perturbation ($\Delta P$, mb) traces over the 16-h period centered on the time of the alongshore wind reversal (from northerly to southerly) at the surface. Trace 1: Measurements based on the composite of the 10–11 June 1994 event shown in Fig. 10 (event composite, solid curve). Trace 2: Measurements calculated hydrostatically from aircraft-observed temperature changes between 70 and 900 m MSL (solid curve with dots) as the aircraft crossed the leading edge of the disturbance (Fig. 3). The four dots (left to right) correspond to the four aircraft ascent soundings in Fig. 3b (recall that the aircraft traveled from left to right in Fig. 3b). The spatial coordinate from the aircraft was transformed into a temporal coordinate by assuming propagation at the observed ground-relative phase speed of 11.9 m $s^{-1}$. Trace 3: The summary of many events at buoys 28 and 13 (vertical bars) from Bond et al. (1996).

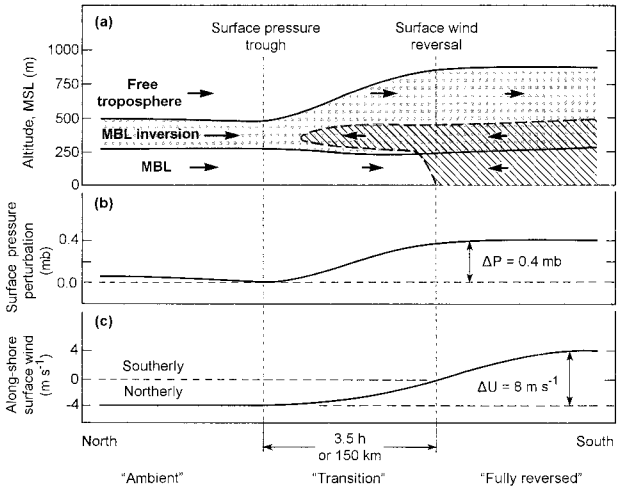


FIG. 12. (a) Schematic summary of the observed vertical structure of the 10–11 Jun 1994 CTD, including the MBL, the temperature inversion capping the MBL (light shading), and the free troposphere above the inversion. The alongshore wind is shown by vectors, and the region of southerly winds is marked by hatching. (b) Surface pressure perturbations and (c) surface alongshore wind perturbations are also shown. Three domains are marked: *ambient*, which represents conditions ahead of the perturbation; *transition*, which marks the region where the perturbation has appeared aloft but the alongshore wind has not reversed at the surface; and *fully reversed*, which marks the region where the alongshore wind has also become southerly at the surface. The spatial and temporal scales that are shown are based on this single well-observed event. However, the perturbation amplitudes ($\Delta P$, surface pressure perturbation; $\Delta U$, surface alongshore wind perturbation) and the phase relationships between perturbations at the surface and aloft are also representative of most CTDs in the region, as is described in the text based on comparison with the climatology of many events presented in Bond et al. (1996).

face pressure signal, but with a different vertical structure, this seems highly unlikely. The vertical structure of this event is summarized in Fig. 12 (based on data presented in Figs. 3, 4, 6, 10, and 11, and on analyses presented in sections 4, 6, and 7). This figure highlights the observed phase relationships between the surface pressure perturbation, the alongshore wind reversal at the surface and aloft, and the upward expansion of the MBL inversion. Although the detailed spatial and temporal scales shown in the schematic are based on the well-observed event of 10–11 June 1994, the key phase relationships and perturbation amplitudes are characteristic of most CTDs, as described above.

The conclusion that the three-layered structure observed in the 10–11 June 1994 event is characteristic of most CTDs brings into question the applicability of the shallow-water equations to the CTD phenomena because the observations have established that the primary perturbation occurs within the very layer that is assumed to be infinitely thin in the shallow-water system. It is the focus of the next section to explore this apparent limitation and to assess the applicability of Kelvin wave and internal bore behavior to the observations of the 10–11 June 1994 CTD.

## 7. Comparison of predicted and observed phase speeds

### *a. Transforming the observed three-layer system into a shallow-water system*

This section considers whether the CTD propagated with a phase speed that is consistent with theoretical expectations for either a Kelvin wave or a bore. However, before this can be done, the observed multilayered structure must be reconciled with the shallow-water system to which the theoretical relationships apply.

To a first-order approximation the thermodynamic observations indicate that CTDs exist in a system consisting of three layers (Fig. 13): an MBL of depth $H$ that remains essentially unperturbed, an MBL inversion (MBLI) of thickness $H_I$ that contains the perturbation, and the free troposphere above. Two primary possibilities appear plausible for transforming this into a quasi-two-layer system: 1) assume the bottom two layers can be considered as the lower layer, with its depth given by the height of the top of the MBL inversion, or 2) assume the top of the MBL acts as a rigid lower boundary and the perturbed layer has a depth given by the thickness of the MBL inversion. In option 1, the MBL

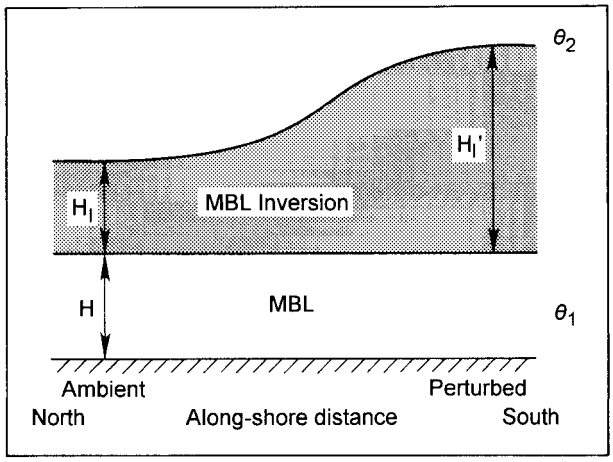


FIG. 13. Schematic overview of the 10–11 Jun 1994 coastally trapped disturbance with features defined for use in the calculation of phase speeds, including depths ($H$, $H_I$, and $H_I'$) and potential temperatures ($\theta_1$ and $\theta_2$). A comprehensive description of these variables is found in Table 2.

and its capping inversion are assumed to respond together within the wave. In option 2, the perturbation is contained entirely within the MBL inversion, an assumption that is closer to the observed behavior than is option 1. However, it remains uncertain why the MBL did not deepen initially while its capping inversion did. It is possible that the lack of strong stratification directly above the inversion provided little resistance to the upward expansion of the upper part of the inversion, while, in contrast, the inversion itself provided strong resistance to the deepening of the MBL beneath it. In either option, each layer is assumed to have a uniform potential temperature given by the mass-weighted potential temperature of each layer.

The intrinsic phase speed of a Kelvin wave (Reason and Steyn 1988, 1992) is given in (1) for a linear Kelvin wave ($c_{\rm LKW}$) and in (2) for a solitary Kelvin wave ($c_{\rm SKW}$). (The solitary wave relationship should apply in cases where the perturbation depth is a significant fraction of the total layer depth.) Equation (2) has been modified from the original form given by Reason and Steyn (1992) by inserting the relationship between the perturbation amplitude and their parameter $\alpha$, described in Reason and Steyn (1988), into Eq. (2.23a) of Reason and Steyn (1992): for option 1 this is given by $\alpha = (H_I' - H_I)/(H_I + H)$, and for option 2, $\alpha = (H_I' - H_I)/(H_I)$. Similarly, the propagation speed relationship for atmospheric internal bores from Klemp et al. (1997) is transformed in Eq. 3 into the system shown in Fig. 13.

*MBL and inversion respond together (option 1):*

$$c_{\rm LKW} = [g'(H + H_I)]^{1/2} \quad (1a)$$

$$c_{\rm SKW} = [g'(H + H_I')]^{1/2} \quad (2a)$$

$$U_{\rm bore} = [2g'(H + H_I')^2/(2H + H_I + H_I')]^{1/2}; \quad (3a)$$

*Only the MBL inversion responds (option 2):*

$$c_{\rm LKW} = [g'(H_I)]^{1/2} \quad (1b)$$

$$c_{\rm SKW} = [g'(H_I')]^{1/2} \quad (2b)$$

$$U_{\rm bore} = [2g'(H_I')^2/(H_I + H_I')]^{1/2} \quad (3b)$$

$$g' = g[(\theta_2 - \theta_1^*)/\theta_2], \quad (4)$$

wherein $g'$ is the reduced gravity, given by (4), where $\theta_I^*$ is the mass-weighted potential temperature of the lower layer as described above for options 1 (i.e., includes both the MBL and its capping inversion) and 2 (i.e., just the inversion), and $\theta_2$ is the potential temperature of the free troposphere above the top of the MBLI, which is assumed here to be the potential temperature of the top of the MBLI. Finally, $g$ is the acceleration due to gravity.

### *b. Calculating theoretical phase speeds from the observations*

In using the observations to determine whether a Kelvin wave or internal bore with the observed perturbation characteristics would have a phase velocity that matches the observed propagation speed, it is necessary to carefully select the heights $H$, $H_I$, and $H_I'$. Uncertainty enters into this selection through observational error, potential temperature analysis errors in the aircraft cross section, the presence of other sources of perturbations in the MBLI, and ambiguity about which potential temperature level best identifies the top and bottom of the MBLI's stable layer. To assess the effects of these uncertainties on the predicted phase velocity, two options for the MBLI top are considered, 306 and 307 K, and the mass-weighted potential temperatures are calculated from the raw (edited) aircraft temperature profiles, which include some slight effects of hysteresis, and from the subjectively analyzed cross section (Fig. 3b). The same ambient and perturbed profiles used to create Figs. 4 and 5 are the basis for these calculations. They are from ascents 140 km apart (Fig. 3b) and were separated by less than 40 min in time. [It should be noted that bore theory assumes that the regions upstream and downstream of the jump are horizontally homogeneous. Although this is well satisfied in the northern, upstream, sounding (note the isentropes in Fig. 3b are horizontal near there), it seems less well satisfied in the southern, downstream, sounding.] The perturbation profiles of Figs. 4 and 5 suggest that the 307-K isentrope better marks the top of the perturbed MBLI than does the 306-K isentrope, so it is emphasized here. The level for which there was no vertical displacement near the top of the MBL was chosen to represent the base of the perturbed layer. This is well defined in the perturbation profiles in Fig. 5 as 265 m MSL, which corresponds to $\theta = 290$ K. However, this level is within the base of the MBLI, about 50–100 m above the top of the MBL.

Based on the conclusion that the disturbance existed

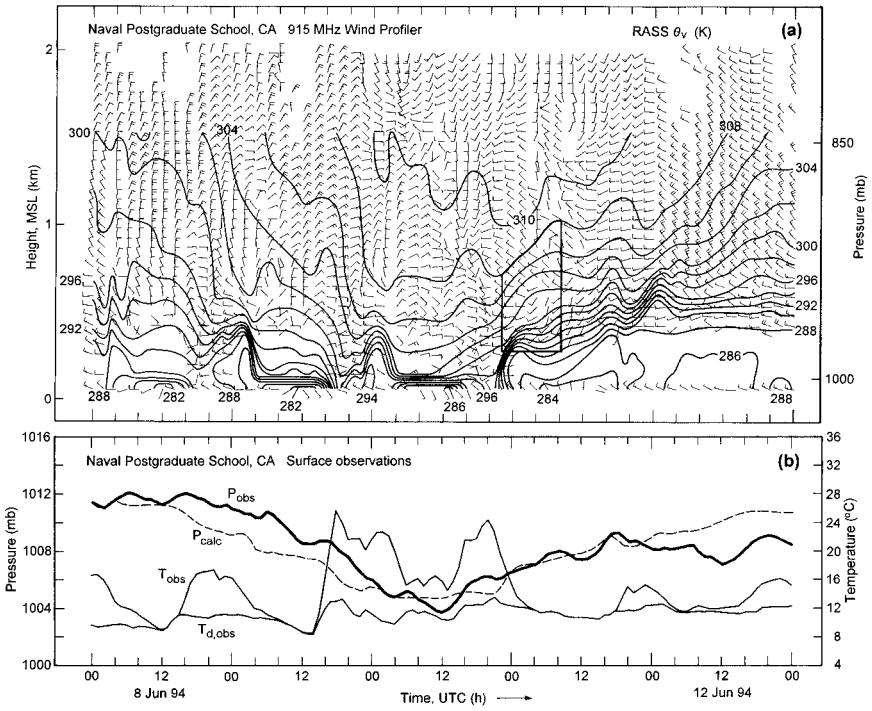


FIG. 14. (a) Time–height section of hourly RASS virtual potential temperature (K, solid) and hourly consensus horizontal winds (vectors as in Fig. 2), from the NPS 915-MHz wind profiler between 0000 UTC 8 and 13 Jun 1994. Hourly averaged surface winds measured at the profiler site are included. The inner bold trapezoid marks the coastally trapped disturbance and is used in calculating phase speeds. For clarity, only every other wind profile is shown. Gaps in profiler data are from interference due to a nearby airport surveillance radar. (b) Surface data from NPS, including observed pressure ($P_{obs}$), temperature ($T_{obs}$), dewpoint temperature ($T_{d,obs}$), and surface pressure calculated hydrostatically from the RASS analysis in (a) below 1.5-km altitude ($P_{calc}$), as described in the text. [Adapted from Ralph et al. (1998).]

offshore in the layer between the 290- and 307-K isentropes, the data from a radar wind profiler and Radio Acoustic Sounding System (RASS) site operated by the Naval Postgraduate School (NPS) near Monterey Bay (Fig. 14) were reexamined for evidence of this perturbation. This provided an independent set of data and, thus, an independent set of predicted phase speeds. Because of the complex terrain in the region and the strong diurnal cycle at that site, the disturbance is masked there to a large degree by these other effects. After including a 1-K adjustment to account for the fact that RASS observed virtual temperature, rather than temperature, it is evident that the layer with virtual potential temperatures ($\theta_v$) from 291 to 308 K broadened vertically in a manner similar to that observed offshore. The perturbation at the NPS profiler–RASS began around 2000 UTC 10 June, 2–3 h after the buoy offshore from Monterey Bay experienced the wind reversal. The upward expansion of the MBLI occurred over about 12 h at NPS between 2000 UTC 10 June and 0800 UTC 11 June, which corresponds roughly to the pause in northward propagation. This transition was slow compared to the 3–4-h time span over which it occurred during the strongly propagating phase, which is consistent with the earlier conclusion that the CTD was approximately stalled at this time by diurnal changes in the background flow. The intrinsic phase speeds for linear and solitary Kelvin waves and internal bores were then calculated from these RASS data (Table 2).

### *c. Comparison of theoretical and observed intrinsic phase speeds*

The resulting intrinsic phase speeds for linear and solitary Kelvin waves, as well as for internal bores, are provided in Table 2 for both transformations of the observed three-layer system into a shallow-water system, that is, options 1 and 2, and for both aircraft- and RASS-based measurements. This is also illustrated and summarized schematically in Fig. 15a. As expected, for a given option, the predicted phase speeds for the bore are greater than for the solitary Kelvin wave, which are greater than for the linear Kelvin wave. Also, because option 2 excludes the MBL from the calculations, it uses layers that have depths less than those in option 1. This results in slower phase speeds for option 2 than for option 1. Overall, the predicted phase speeds vary between 9.2 and 18.3 m $s^{-1}$, and have uncertainties of

TABLE 2. Observed parameters as well as predicted Kelvin wave and internal bore intrinsic phase speeds for the 10–11 Jun 1994 coastally trapped disturbance. The observed intrinsic phase speed, which is based on a ground-relative phase speed of 11.9 ± 0.3 m s$^{-1}$ and an estimated opposing flow of 1.3 ± 0.3 m s$^{-1}$, is used for comparison. Linear Kelvin wave phase speeds ($c_{LKW}$), solitary Kelvin wave phase speeds ($c_{SKW}$), and internal bore phase speeds ($U_{bore}$) are shown. $H$ is the depth of the marine boundary layer, $H_I$ is the ambient MBL inversion thickness, $H_I'$ is the perturbed MBL inversion thickness, $\theta_1$ is the average potential temperature of the MBL, $\theta_2$ is the potential temperature of the inversion top, $\theta_1^*$ is the mass-weighted potential temperature of the inversion (option 2) or of the combination of the MBL and inversion (option 1), $g' = g\,[(\theta_2 - \theta_1^*)/\theta_2]$ is the reduced gravity, and $g$ is the acceleration due to gravity.

| | | | | | | | MBL and MBLI behave as one layer (option 1) | | | MBL behaves as a rigid lower boundary (option 2) | | |
|---|---|---|---|---|---|---|---|---|---|---|---|---|
| Data source | $H$ (m) | $H_I$ (m) | $H_I'$ (m) | $\theta_1$ (K) | $\theta_1^*$[a] (K) | $\theta_2$ (K) | $c_{LKW}$[b] (m s$^{-1}$) | $c_{SKW}$[c] (m s$^{-1}$) | $U_{bore}$[d] (m s$^{-1}$) | $c_{LKW}$[e] (m s$^{-1}$) | $c_{SKW}$[f] (m s$^{-1}$) | $U_{bore}$[g] (m s$^{-1}$) |
| Raw aircraft data (edited) | 265 | 361 | 535 | 286 | 300.2 | 306 | 15.5 | 16.4 | 17.4 | 8.2 | 10.0 | 10.9 |
| | 265 | 460 | 635 | 286 | 301.2 | 307 | 16.2 | 17.2 | 18.1 | 9.2 | 10.8 | 11.7 |
| Subjective $\theta$ analysis of aircraft data in cross section | 265 | 375 | 615 | 286 | 299.4 | 306 | 15.8 | 17.3 | 18.6 | 8.9 | 11.4 | 12.7 |
| | 265 | 520 | 735 | 286 | 300.6 | 307 | 16.8 | 18.1 | 19.2 | 10.3 | 12.2 | 13.2 |
| NPS RASS virtual temperature | 265 | 440 | 760 | 287 | 301.2 | 308 | 16.5 | 18.5 | 20.1 | 9.8 | 12.9 | 14.4 |
| (Average of four aircraft-based estimates) | | | | | | | (16.1 ± 0.6) | (17.2 ± 0.7) | (18.3 ± 0.8) | (9.2 ± 0.9) | (11.1 ± 0.9) | (12.1 ± 1.0) |
| All five estimates | | | | | | | 16.2 ± 0.5 | 17.5 ± 0.8 | 18.7 ± 1.0 | 9.3 ± 0.8 | 11.5 ± 1.1 | 12.6 ± 1.4 |
| Difference from the observed intrinsic phase speed of 13.2 ± 0.6 m s$^{-1}$ | | | | | | | 3.0 | 4.3 | 5.5 | −3.9 | −1.7 | −0.6 |

[a] For option 2 $\theta_1^*$ is given in the table; $\theta_1^*$ for option 1 can be calculated, using $\theta_1^*$, $H$, $H_I$, $H_I'$, and $\theta_1$, as given in the table, from $[H\theta_1 + H_I\theta_1^*]/(H + H_I)$ for $c_{LKW}$ and from $[H\theta_1 + H_I'\theta_1^*]/(H + H_I')$ for $c_{SKW}$ and $U_{bore}$.

[b] $c_{LKW} = \sqrt{g'\,(H_I + H)}$.

[c] $c_{SKW} = \sqrt{g'\,(H_I' + H)}$.

[d] $U_{bore} = \sqrt{2g'\,(H + H_I')^2/(2H + H_I + H_I')}$.

[e] $c_{LKW} = \sqrt{g'\,(H_I)}$.

[f] $c_{SKW} = \sqrt{g'\,(H_I')}$.

[g] $U_{bore} = \sqrt{2g'\,(H_I')^2/(H_I + H_I')}$.

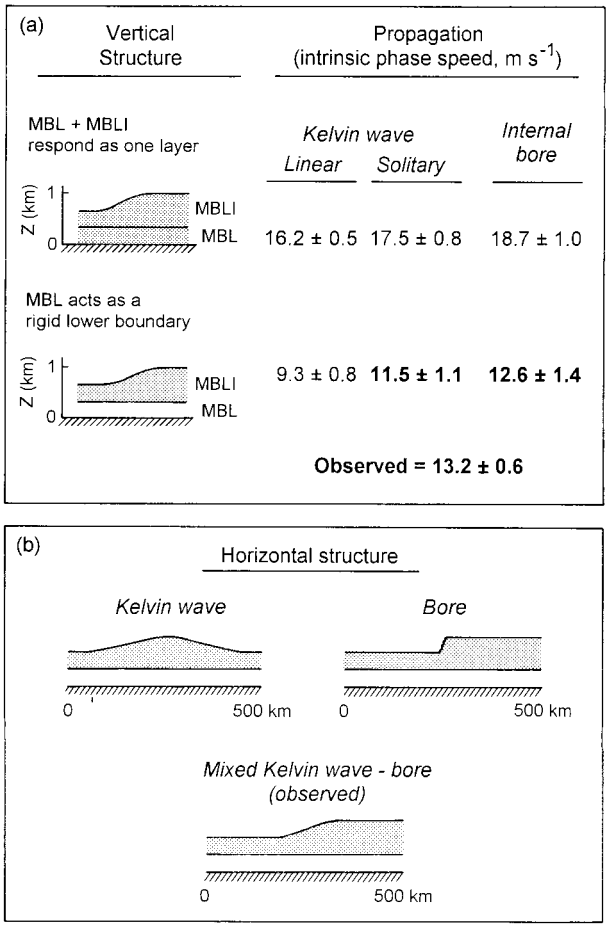


FIG. 15. Summary of predicted and observed behavior in the 10–11 Jun 1994 coastally trapped disturbance. (a) Comparison of predicted and observed intrinsic phase speeds based on assumptions concerning the dynamical mechanisms responsible (i.e., either linear or solitary Kelvin wave or internal bore) for the CTD, and on whether the MBLI responded alone, with the MBL acting as a rigid lower boundary, or the two layers responded together. (b) Comparison of the observed alongshore variations of the disturbance's vertical structure with those expected for a linear or solitary Kelvin wave, or a bore.

0.5–1.4 m $s^{-1}$ based on the availability of five estimates for each type of disturbance and each option. The spread of these predicted phase speeds over roughly a factor of 2 suggests that in this case the phase speed may be a useful indicator of the dynamics, especially because the uncertainty in the observed intrinsic phase speed is relatively small (0.6 m $s^{-1}$). This inference is also supported by the fact that the uncertainty in each estimated phase speed ($<$1.5 m $s^{-1}$) is much less than the total range of predicted phase speeds (9.1 m $s^{-1}$).

From Table 2 it is apparent that the predicted phase speeds for option 1 are all too high by a significant amount. In contrast, the predicted phase speeds for option 2 are somewhat less than the observed phase speed. However, the predicted phase speeds for both the bore and the solitary Kelvin wave in option 2 are within the uncertainties. Of these, the bore is slightly closer (0.6 m $s^{-1}$) to the observed phase speed than is the solitary Kelvin wave (1.7 m $s^{-1}$). If it is assumed under option 1 that the entire layer from the surface to the top of the MBLI has the potential temperature of the MBL, the predicted phase speeds would be even greater. It is useful to note that the best quantitative agreement is for conditions that appeared to best describe the conditions qualitatively, that is, the relatively unperturbed depth of the MBL implied that it was not directly incorporated in the disturbance, and the significant amplitude implied that nonlinearities would be important.

### *d. Limitations of Kelvin wave and bore theories with respect to the observed event*

Because the theoretical relationships for phase speed in these theories depend explicitly only on the thermodynamic and geometric (layer depths) characteristics of the CTD and its environment, the above analysis goes to great lengths to address the uncertainties of the predicted phase speeds as a function of uncertainties in these variables. However, the kinematic structure of these disturbances is an integral part of the phenomenon and is in fact the basis upon which CTDs are defined (i.e., a reversal in the alongshore wind). This section points out some possibly important differences between the observed kinematic structure and that associated with the theories.

These theories are derived from the shallow-water equations in which the velocities represent layer averages, and it is usually assumed that little vertical shear is present. In this respect, the jetlike structure of the wind profile both ahead of and within the observed disturbance indicates the presence of vertical shear (Fig. 6). This is also reflected in the fact that the vertical structure of the observed alongshore wind perturbation is different than the thermodynamic structure. The wind perturbation is greatest in the lowest 400 m MSL while the thermodynamic perturbation is greatest above that (Fig. 5; section 4). However, wind profiler data (Fig. 9) do indicate that the vertical shear of the composite diurnal cycle, which is a measure of the shear in the CTD environment, is very small ($<$1 m $s^{-1}$ $km^{-1}$) during the propagating phase and roughly 4 m $s^{-1}$ $km^{-1}$ during the stalled phase. In addition, the most representative single profile ahead of the CTD (''ambient'' in Fig. 6a) shows substantial shear between the MBL and its capping inversion, but that the shear in the inversion itself is rather small.

The observation of relatively strong cross-shore wind perturbations (Fig. 6b) is another aspect of the kinematics that is not easily reconciled with the bore and Kelvin wave theories. Although solitary Kelvin wave theory does allow for weak cross-shore winds, both the linear Kelvin wave and bore theories assume zero cross-shore winds.

Thus, although the thermodynamic and phase speed

characteristics fit the theory well, based on the MBL acting as a quasi-rigid lower boundary, the kinematic structure of the CTD and its environment does not fit readily into this interpretation, except in the important sense that the kinematic perturbation appeared first in the inversion rather than at the surface (Fig. 3b).

## 8. Conclusions

Based upon the uniquely detailed and comprehensive measurements of a CTD gathered during a field experiment along the California coast on 10–11 June 1994, an analysis was performed both to assess the representativeness of this single event to other CTDs and to explore its dynamical nature. Aircraft data were used to document the vertical and horizontal structure of the CTD, including the fact that there was a node in the vertical displacements near 250 m MSL (a position just above the base of the inversion capping the MBL) above which the displacements were upward and below which they were downward. It was also established that the wind direction reversed first aloft from northerly to southerly, and then at the surface, and that the cross-shore winds were directed onshore within the northerlies and offshore within the southerlies. The alongshore wind shifted by 7.8 m $s^{-1}$ on average at the surface, and by up to 10 m $s^{-1}$ at the base of the inversion. The cross-shore wind shifted by 2.4 m $s^{-1}$ at the surface and by 6 m $s^{-1}$ aloft. Overall, these observations establish that the CTD thermodynamic perturbations were most pronounced within the capping inversion, rather than at the surface, as had been shown in Ralph et al. (1998) in less detail. However, the alongshore wind perturbation is generally stronger in the MBL than in the inversion and is strongest at the base of the inversion.

The observed variations of wind and surface pressure in a composite of measurements at several buoys in the 10–11 June 1994 CTD were compared with the climatology of many CTDs at several buoys along the U.S. west coast given in Bond et al. (1996). This established that the surface perturbations were consistent with a ''typical'' CTD. The 1994 CTD included the presence of a pressure trough 3.0 $\pm$ 0.5 h before the reversal of the alongshore wind direction and a 0.42 $\pm$ 0.04 mb pressure rise between the trough and the time of the wind shift. This is based on hydrostatic surface pressure perturbations derived from aircraft data (0.47-mb rise over 2.4 h) and a composite of the event derived from buoy data (0.38-mb rise over 3.5 h). This compares very well with the average behavior of many CTDs at buoys 28 and 13 studied in Bond et al. (1996), for which the trough led the wind shift by 3.5 $\pm$ 0.5 h, and the pressure rose by 0.40 $\pm$ 0.08 mb between the time the trough passed and time that the along-shore wind direction reversed. An assessment was then made of the universality of the observation that the CTD perturbation appeared first in the inversion above the surface before the surface wind direction shifted. The aircraft data were used to show that the surface pressure changes resulting from cooling associated with the upward displacements within the inversion were nearly identical to the pressure changes observed at the surface. This is strong evidence that the surprising vertical structure observed in the 10–11 June 1994 CTD is representative of most CTDs in the area. The favorable comparison between the aircraft-derived pressure perturbations and the event composite also supports the conclusion that the upward thickening of the MBL inversion (even though it was observed by aircraft only when the CTD was stalled in its northward propagation) did propagate in connection with the surface wind reversal.

This result indicates that the shallow-water system of equations that has traditionally been applied to this problem may be too simplified to capture essential aspects of the observed structure. This possible limitation was explored using two hypotheses as bases for reconciling the observed three-layer structure with the shallow-water system: 1) the MBL and its capping inversion responded as one layer with a depth given by the height of the top of the inversion, and 2) the inversion responded alone while the MBL acted as a rigid lower boundary. These concepts were tested through their implications regarding the phase speeds of linear and solitary Kelvin waves as well as internal bores. Note that the solitary wave is a special form of nonlinear Kelvin wave for which theory provides a prediction of the phase speed. For this reason, it is used here to illustrate the important differences between linear and nonlinear Kelvin waves in terms of their phase speeds. Comparison of the predicted and observed intrinsic phase speeds indicated that the MBL acted as a rigid lower boundary for the CTD to propagate within the inversion, and that the observed propagation was consistent with either a nonlinear (solitary) Kelvin wave or an internal bore. This ambiguity is also present in the observed alongshore structure, as illustrated in Fig. 15b. On the one hand, the observed disturbance most closely resembles a bore in the sense that the upward perturbation does not return to the ambient state as expected in a wave of elevation (see Skamarock et al. 1996). On the other hand, the slope of the perturbation is gradual as expected for a wave, but not for a bore, which is often referred to as a ''jump'' because it is so abrupt. The abruptness is an important factor because it is related to the production of turbulence, the vertical distribution of which influences the propagation of a bore (Klemp et al. 1997). While the observed perturbation consisted of a slope of approximately 1/300, the slope in a bore is closer to ⅓ (e.g., Rotmann and Simpson 1989; Klemp et al. 1997).

Thus, both the structure and the propagation of the 10–11 June 1994 CTD have characteristics that are best interpreted as a hybrid between an internal bore and a nonlinear Kelvin wave, suggesting that it should be referred to as a *mixed Kelvin wave–bore.* A possible explanation for this result could lie in the fact that the steepening of a Kelvin wave could ultimately lead to a

shocklike disturbance as suggested by Reason and Steyn (1992). It is also plausible to speculate that the energy loss to the upper layer that is required to properly account for the propagation of an internal bore could occur through upward emanation of energy by gravity waves, rather than by the turbulence that has traditionally been considered (Klemp et al. 1997). If the gravity wave emanation became effective at smaller slopes than those required to develop turbulence, then the observed shallow slope could still be consistent with that in an internal bore. This paper suggests that CTDs could be added to the list of atmospheric phenomena that are best characterized as a hybrid of otherwise distinct phenomena, including the *mixed Rossby–gravity wave* and *isolated propagating flows*, the later of which was recently shown to involve both density-driven and wave-dominated effects (Manasseh et al. 1998).

*Acknowledgments.* We acknowledge three anonymous reviewers for their useful and insightful comments, which led to a significantly improved manuscript. We thank Dr. Nick Bond (JISAO/University of Washington) for providing the digital files containing the climatology of buoy data during CTDs, which was used in creating Fig. 11. Figures were expertly drafted by Jim Adams.

## REFERENCES

Bane, J. M., S. M. Haines, L. Armi, and M. H. Sessions, 1995: The California coastal marine layer: Winds and thermodynamics, June 1994 aircraft measurement program. Tech. Rep. CMS-95-1, 289 pp. [Available from University of North Carolina, Chapel Hill, NC 27599-3300.]

Banta, R. M., 1995: Sea breezes shallow and deep on the California coast. *Mon. Wea. Rev.,* **123,** 3614–3622.

Beardsley, R. C., C. E. Dorman, C. A. Friehe, L. K. Rosenfeld, and C. D. Winant, 1987: Local atmospheric forcing during the coastal ocean dynamics experiment, 1. A description of the marine boundary layer and atmospheric conditions over a northern California upwelling region. *J. Geophys. Res.,* **92,** 1467–1488.

Benjamin, T. B., 1968: Gravity currents and related phenomena. *J. Fluid Mech.,* **31,** 209–248.

Bond, N. A., C. F. Mass, and J. E. Overland, 1996: Coastally trapped wind reversals along the United States west coast during the warm season. Part I: Climatology and temporal evolution. *Mon. Wea. Rev.,* **124,** 430–445.

Dorman, C. E., 1985: Evidence of Kelvin waves in California's marine layer and related eddy generation. *Mon. Wea. Rev.*, **113,** 827–839.

——, 1987: Possible role of gravity currents in northern California's coastal summer wind reversals. *J. Geophys. Res.*, **92,** 1497–1506.

Gill, A. E., 1977: Coastally trapped waves in the atmosphere. *Quart. J. Roy. Meteor. Soc.*, **103,** 431–440.

——, 1982: *Atmosphere–Ocean Dynamics.* Academic Press, 662 pp.

Hermann, A. J., B. M. Hickey, C. M. Mass, and M. D. Albright, 1990: Orographically trapped coastal wind events in the Pacific Northwest and their oceanic response. *J. Geophys. Res.,* **95,** 13 169–13 193.

Holt, T. R., 1996: Mesoscale forcing of a boundary layer jet along the California coast. *J. Geophys. Res.,* **101,** 4235–4254.

Houghton, D. D., and A. Kasahara, 1968: Nonlinear shallow fluid flow over an isolated ridge. *Commun. Pure Appl. Math.,* **21,** 1–23.

Klemp, J. B., R. Rotunno, and W. C. Skamarock, 1997: On the propagation of internal bores. *J. Fluid Mech.,* **331,** 81–106.

Manasseh, R., C.-Y. Ching, and H. J. S. Fernando, 1998: The transition from density-driven to wave-dominated isolated flows. *J. Fluid Mech.,* **361,** 253–274.

Mass, C. F., 1995: Comments on ''The dynamics of coastally trapped mesoscale ridges in the lower atmosphere.'' *J. Atmos. Sci.,* **52,** 2313–2318.

——, and M. D. Albright, 1987: Coastal southerlies and alongshore surges of the west coast of North America: Evidence of mesoscale topographically trapped response to synoptic forcing. *Mon. Wea. Rev.,* **115,** 1707–1738.

——, and N. A. Bond, 1996: Coastally trapped wind reversals along the United States west coast during the warm season. Part II: Synoptic evolution. *Mon. Wea. Rev.,* **124,** 446–461.

Neiburger, M., D. S. Johnson, and C. W. Chien, 1961: Studies of the structure of the atmosphere over the eastern North Pacific Ocean. Part I: The inversion over the eastern North Pacific Ocean. *Univ. Calif. Publ. Meteor.,* **1,** 1–94.

Nuss, W. A., and D. W. Titley, 1994: Use of multiquadric interpolation for meteorological objective analysis. *Mon. Wea. Rev.,* **122,** 1611–1631.

Ralph, F. M., L. Armi, J. M. Bane, C. Dorman, W. D. Neff, P. J. Neiman, W. Nuss, and P. O. G. Persson, 1998: Observations and analysis of the 10–11 June 1994 coastally trapped disturbance. *Mon. Wea. Rev.*, **126,** 2435–2465.

Reason, C. J. C., and D. G. Steyn, 1988: Comments on ''Diffraction of solitary Kelvin waves at Cape Mendocino.'' *Mon. Wea. Rev.*, **116,** 804–805.

——, and ——, 1992: The dynamics of coastally trapped mesoscale ridges in the lower atmosphere. *J. Atmos. Sci.,* **49,** 1677–1692.

——, and ——, 1995: Reply. *J. Atmos. Sci.,* **52,** 2319–2324.

Rogerson, A. M., and R. M. Samelson, 1995: Synoptic forcing of coastal-trapped disturbances in the marine atmospheric boundary layer. *J. Atmos. Sci.,* **52,** 2025–2040.

Rottman, J. W., and J. E. Simpson, 1989: The formation of internal bores in the atmosphere: A laboratory model. *Quart. J. Roy. Meteor. Soc.*, **115,** 941–963.

Samelson, R. M., and A. M. Rogerson, 1996: Life cycle of a linear coastally trapped disturbance. *Mon. Wea. Rev.*, **124,** 1853–1863.

Simpson, J. E., 1987: *Gravity Currents in the Environment and the Laboratory.* Ellis Horwood, 244 pp.

Skamarock, W. C., J. B. Klemp, and R. Rotunno, 1996: The diffraction of Kelvin waves and bores at coastal bends. *J. Atmos. Sci.,* **53,** 1327–1337.

Thompson, W. T., T. Haack, J. D. Doyle, and S. D. Burke, 1997: A nonhydrostatic mesoscale simulation of the 10–11 June 1994 coastally trapped wind reversal. *Mon. Wea. Rev.,* **125,** 3211–3230.

Winant, C. D., C. E. Dorman, C. A. Friehe, and R. C. Beardsley, 1988: The marine layer off northern California: An example of supercritical channel flow. *J. Atmos. Sci.,* **45,** 3588–3605.